Image Reconstruction in Optical Interferometry

Éric Thiébaut

Image Reconstruction in Optical Interferometry

É. Thiébaut

Centre de Recherche Astrophysique de Lyon, CNRS/UMR 5574, Observatoire de Lyon, Université Lyon 1, École Normale Supérieure de Lyon – 9, avenue Charles André – 69561 Saint Genis Laval Cedex – France

thiebaut@obs.univ-lyon1.fr

Abstract: Inverse problem approach is a suitable framework to analyze the challenging issues in image reconstruction from interferometric data. It can be exploited to describe and formally compare the new methods specifically developed for optical interferometry.

OCIS codes: 100.0100, 100.3175.

1. Optical Interferometry

Optical multi-telescope interferometers provide sparse measurements of the Fourier transform $\hat{I}_\lambda(\boldsymbol{\nu})$ of $I_\lambda(\boldsymbol{\theta})$, the specific brightness distribution of the observed object in angular direction $\boldsymbol{\theta}$ and at wavelength λ. Indeed, at instant t, the complex visibility of the fringe pattern of interferences between the telescopes j_1 and j_2 is:

$$V_{j_1,j_2}(t) = g^\star_{j_1}(t)\, g_{j_2}(t)\, \hat{I}_\lambda\Big(\boldsymbol{\nu}_{j_1,j_2}(t)\Big) \quad \text{with} \quad \boldsymbol{\nu}_{j_1,j_2}(t) = \frac{\boldsymbol{r}_{j_2}(t) - \boldsymbol{r}_{j_1}(t)}{\lambda}, \tag{1}$$

with $g_j(t)$ and $\boldsymbol{r}_j(t)$ the complex amplitude transmission and the projected position (on a plane perpendicular to the line of sight) of the j-th telescope. Averaging during an exposure (assumed short enough to neglect the Earth rotation) yields:

$$V_{j_1,j_2,m} = \langle V_{j_1,j_2}(t)\rangle_m \simeq \langle g^\star_{j_1}(t)\, g_{j_2}(t)\rangle_m\, \hat{I}_\lambda(\boldsymbol{\nu}_{j_1,j_2,m}) \quad \text{with} \quad \boldsymbol{\nu}_{j_1,j_2,m} = \langle \boldsymbol{\nu}_{j_1,j_2}(t)\rangle_m, \tag{2}$$

where $\langle\rangle_m$ denotes time averaging during m-th exposure. At optical wavelengths, the optical path variations due to the turbulence involve that $\langle g^\star_{j_1}(t)\, g_{j_2}(t)\rangle_m \simeq 0$. In other words, complex visibilities cannot be directly measured. To overcome this issue, other quantities such as the powerspectrum and the bispectrum are measured:

$$S_{j_1,j_2,m} = \langle |V_{j_1,j_2}(t)|^2\rangle_m \simeq \rho_{j_1,m}\,\rho_{j_2,m}\,|\hat{I}_\lambda(\boldsymbol{\nu}_{j_1,j_2,m})|^2, \tag{3}$$

$$B_{j_1,j_2,j_3,m} = \langle V_{j_1,j_2}(t)\, V_{j_2,j_3}(t)\, V_{j_3,j_1}(t)\rangle_m \simeq \rho_{j_1,m}\,\rho_{j_2,m}\,\rho_{j_3,m}\,\hat{I}_\lambda(\boldsymbol{\nu}_{j_1,j_2,m})\,\hat{I}_\lambda(\boldsymbol{\nu}_{j_2,j_3,m})\,\hat{I}_\lambda(\boldsymbol{\nu}_{j_3,j_1,m}), \tag{4}$$

where $\rho_{j,m} = \langle |g_j(t)|^2\rangle_m \neq 0$ can be calibrated from photometric channels and a reference source. Of particular interest is the phase of the bispectrum, the so-called *phase closure*, since it is more robust to calibration errors.

2. Image Synthesis

The first problem in image reconstruction from interferometric data is to cope with voids in the sampled spatial frequencies (see Fig. 1a for a typical coverage of the measured spatial frequencies). At optical wavelengths, working with the powerspectrum and bispectrum data gives less Fourier phase information and introduces non-linearities and degeneracies which make the image synthesis problem much more difficult. Nevertheless and without loss of generality, image synthesis from interferometric data is an inverse problem [1] that can be restated as a constrained minimization [2, 3] to find the best image parameters, *e.g.* the *pixel* intensities, $\boldsymbol{x}$:

$$\boldsymbol{x}^+ = \underset{\boldsymbol{x}\in\mathscr{X}}{\arg\max}\Big\{f_{\text{data}}(\boldsymbol{x},\boldsymbol{y}) + f_{\text{prior}}(\boldsymbol{x})\Big\} \quad \text{with, } \textit{e.g.}, \quad \mathscr{X} = \Big\{\boldsymbol{x}\,|\,\boldsymbol{x}\geq 0, \sum\nolimits_k x_k = 1\Big\} \tag{5}$$

with $f_{\text{data}}(\boldsymbol{x},\boldsymbol{y})$ a likelihood term (usually derived from the statistics of the noise) which enforces agreement with the measurements $\boldsymbol{y}$, and $f_{\text{prior}}(\boldsymbol{x})$ a regularization term which imposes some regularity, *e.g.* smoothness, for the

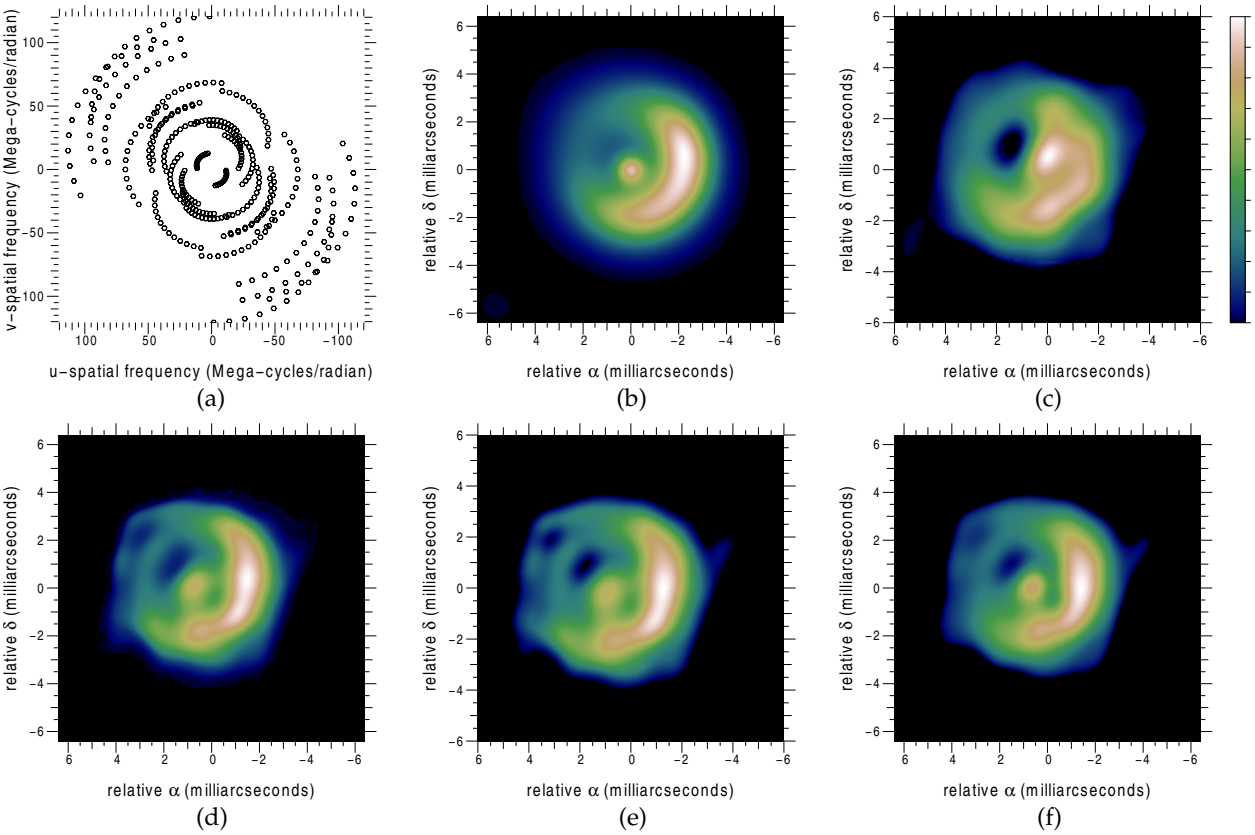

Fig. 1: **(a)** Spatial frequency coverage. **(b)** Original object smoothed to the resolution of the interferometer (FWHM ~ 15 mas). **(c)** Image reconstruction without any Fourier phase information. Image reconstruction with various types of regularization: **(d)** reconstruction with maximum entropy regularization as in Eq. (6); **(e)** reconstruction with edge-preserving regularization as in Eq. (7); **(f)** reconstruction with a quadratic regularization given by Eq. (8) and which imposes a compact field of view. All reconstructions by algorithm MiRA [4] and from the powerspectrum and the phase closures.

sought image. Other strict constraints such as the non-negativity and normalization are imposed by requiring that $\boldsymbol{x}$ belongs to a feasible set $\mathscr{X}$.

In this general framework, an image reconstruction algorithm is specified by: (i) the image representation (*e.g.* pixels, *building-blocks* [5], ...) and its Fourier transform; (ii) the approximation of the likelihood (*e.g.* [6]); (iii) the imposed constraints (type of regularization, non-negativity, normalization, *etc.*); and (iv) the optimization strategy. Different choices for these ingredients have led to a variety of algorithms. For instance, Maximum Entropy Methods (MEM) [7] readily solve a problem like the one Eq. (5) with a regularization:

$$f_{\text{prior}}(\boldsymbol{x}) = \sum\nolimits_n \left[x_n \log(x_n/\bar{x}_n) - x_n + \bar{x}_n \right] \tag{6}$$

with $\bar{\boldsymbol{x}}$ the *default image* (*cf.* Fig. 1d). BSMEM [8] is a version of MEM applied to bispectral data. CLEAN [9] uses a *matching-pursuit* algorithm to minimize the number of point-like sources that compose the image. This is very like the sparsity constraints used in *Compressive Sensing* [10] and expressed as: $f_{\text{prior}}(\boldsymbol{x}) = \|\boldsymbol{x}\|_1$ to minimize the ℓ_1-norm of the parameters. The *building-block* method [5] can be seen as an adaptation of CLEAN to bispectral data. Imposing the sparsity of the spatial gradient of the image, a method known as *Total Variation* (TV) [11], or an edge preserving smoothness regularization is obtained with:

$$f_{\text{prior}}(\boldsymbol{x}) = \sum\nolimits_n \left[\sqrt{\|\nabla_n \boldsymbol{x}\|^2 + \epsilon^2} - \epsilon \right], \tag{7}$$

with $\varepsilon = 0$ for TV, $\varepsilon > 0$ otherwise and $\|\nabla_n \boldsymbol{x}\|$ the image gradient at n-th pixel. When $\varepsilon \to \infty$, Eq. (7) yields

quadratic smoothness which is the regularization used by WIPE [12]. More recently, a simple separable quadratic regularization has proven to be successful for optical interferometry imaging [13]:

$$f_{\text{prior}}(\boldsymbol{x}) = \sum\nolimits_n w_n x_n^2, \tag{8}$$

with the weights $w_n \geq 0$ set so as to favor the concentration of the light near the center of the field of view and hence the smoothness of $\hat{I}_\lambda(\boldsymbol{\nu})$. This flexibility is exploited by versatile algorithms like MiRA [4] or WISARD [14] which implement various kind of regularizations and can therefore emulate other algorithms (their however differ in their optimization strategies). Comparing the results obtained with different regularizations (*cf.* Fig. 1d-f) shows that the reconstructed images are very similar and close to the true object. This consistency is reassuring but deserves a quantitative comparison on the impact of the type of regularizations on a variety of cases.

An other advantage of the inverse approach is that the problem in Eq. (5) yields a solution whatever is the amount of missing data (though the less data the less information is gained with respect to the priors). For instance, apart for a 180° ambiguity in the orientation, an image may be synthesized without any measured Fourier phase information (see Fig. 1c for an example of reconstruction).

For the moment, no algorithms really exploit the full potential of the multi-spectral data provided by optical interferometers. Either the object is considered as *gray* with the same distribution at all wavelengths, or a monochromatic image is synthesized for each spectral channel independently [15]. The most exciting developments in image reconstruction algorithms for the years to come will be to use the spectral continuity of the sought brightness distribution to globally process all available data to produce a full 3-D distribution $I_\lambda(\boldsymbol{\theta})$.

References

1. A. Tarantola, *Inverse Problem Theory and Methods for Model Parameter Estimation* (SIAM, 2005).
2. É. Thiébaut, "Image reconstruction with optical interferometers," New Astronomy Reviews **53**, 312–328 (2009).
3. É. Thiébaut and J.-F. Giovannelli, "Image Reconstruction in Optical Interferometry," IEEE Signal Processing Magazine **27**, 97–109 (2010).
4. É. Thiébaut, "MiRA: an effective imaging algorithm for optical interferometry," in "Astronomical Telescopes and Instrumentation," , vol. 7013, F. D. M. Schöller, W. C. Danchi, ed. (SPIE, 2008), vol. 7013, pp. 70,131I–1–70,131I–12.
5. K.-H. Hofmann and G. Weigelt, "Iterative image reconstruction from the bispectrum," Astron. & Astrophys.**278**, 328–339 (1993).
6. S. Meimon, L. M. Mugnier, and G. le Besnerais, "Convex approximation to the likelihood criterion for aperture synthesis imaging," J. Opt. Soc. Am. A **22**, 2348–2356 (2005).
7. R. Narayan and R. Nityananda, "Maximum entropy image restoration in astronomy," Annual Rev. of Astron. & Astrophys.**24**, 127–170 (1986).
8. D. F. Buscher, "Direct maximum-entropy image reconstruction from the bispectrum," in "IAU Symp. 158: Very High Angular Resolution Imaging," , J. G. Robertson and W. J. Tango, eds. (1994), pp. 91–+.
9. J. A. Högbom, "Aperture Synthesis with a Non-Regular Distribution of Interferometer Baselines," Astron. & Astrophys. Suppl.**15**, 417–426 (1974).
10. E. J. Candes, J. Romberg, and T. Tao, "Robust uncertainty principles: exact signal reconstruction from highly incomplete frequency information," IEEE Transactions on Information Theory **52**, 489– 509 (2006).
11. D. Strong and T. Chan, "Edge-preserving and scale-dependent properties of total variation regularization," Inverse Problems **19**, S165–S187 (2003).
12. A. Lannes, "Weak-phase imaging in optical interferometry," J. Opt. Soc. Am. A **15**, 811–824 (1998).
13. G. le Besnerais, S. Lacour, L. M. Mugnier, E. Thiébaut, G. Perrin, and S. Meimon, "Advanced Imaging Methods for Long-Baseline Optical Interferometry," IEEE Journal of Selected Topics in Signal Processing **2**, 767–780 (2008).
14. S. Meimon, L. M. Mugnier, and G. le Besnerais, "Reconstruction method for weak-phase optical interferometry," Optics Letters **30**, 1809–1811 (2005).
15. J.-B. le Bouquin, S. Lacour, S. Renard, É. Thiébaut, and A. Merand, "Pre-maximum spectro-imaging of the Mira star T Lep with AMBER/VLTI," Astron. & Astrophys.**496**, L1–L4 (2009).